Propagation of sound and supersonic bright solitons in superfluid Fermi gases in BCS-BEC crossover

Wen Wen,[1] Shun-Qing Shen,[2] and Guoxiang Huang[3,4,*]

[1]*Department of Physics, East China Normal University, Shanghai 200062, China*
[2]*Department of Physics, University of Hong Kong, Pokfulam Road, Hong Kong, China*
[3]*State Key Laboratory of Precision Spectroscopy and Department of Physics, East China Normal University, Shanghai 200062, China*
[4]*Institute of Nonlinear Physics and Department of Physics, Zhejiang Normal University, Zhejiang 321004, China*

We investigate the linear and nonlinear sound propagations in a cigar-shaped superfluid Fermi gas with a large particle number. We first solve analytically the eigenvalue problem of linear collective excitations and provide explicit expressions of all eigenvalues and eigenfunctions, which are valid for all superfluid regimes in the Bardeen-Cooper-Schrieffer-Bose-Einstein condensation (BCS-BEC) crossover. The linear sound speed obtained agrees well with that of a recent experimental measurement. We then consider a weak nonlinear excitation and show that the time evolution of the excitation obeys a Korteweg de Vries equation. Different from the result obtained in quasi-one-dimensional case studied previously, where subsonic dark solitons are obtained via the balance between quantum pressure and nonlinear effect, we demonstrate that bright solitons with supersonic propagating velocity can be generated in the present three-dimensional system through the balance between a waveguidelike dispersion and the interparticle interaction. The supersonic bright solitons obtained display different physical properties in different superfluid regimes and hence can be used to characterize superfluid features of the BCS-BEC crossover.

PACS number(s): 03.75.Kk, 03.75.Lm, 47.37.+q

I. INTRODUCTION

The remarkable experimental realization of the crossover from a Bardeen-Cooper-Schrieffer (BCS) superfluid to a Bose-Einstein condensation (BEC) in ultracold fermionic atomic gases of ^{6}Li or ^{40}K has provided a new type of macroscopic quantum fluids, and led an enormous progress on the study of trapped, strongly interacting fermions.[1] Of particular interest in this field is the dynamical property of ultracold fermionic atomic gases in various superfluid regimes, including linear collective excitations[1–28], vortices,[29,30] and solitons.[31,32]

For a cigar-shaped condensate, axial excitations can be generally divided into two classes. The first one is the large-size excitation with its spatial extension the same order of the axial length of condensate, which has been intensively studied both theoretically and experimentally in recent years.[2–22] The second one is the small-size excitation that has a spatial extension much less than the axial length of the condensate. The second-class excitations, usually related in particular to sound propagation in the system, have, however, been less investigated up to now.[23–27] Recently, Joseph *et al.*[28] have carried out a beautiful experimental measurement of sound speed in a superfluid ^{6}Li atomic gas in various regimes of the BCS-BEC crossover.

In a recent work, linear and nonlinear excitations in a superfluid Fermi gas has been considered based on a superfluid order-parameter equation valid in the BCS-BEC crossover at zero temperature.[32] The Bogoliubov excitation spectrum for linear sound propagation and subsonic dark solitons have been obtained under a quasi-one-dimensional (Q1D) condition, i.e.,

$$\hbar\omega_\perp \gg \mu_g \gg \hbar\omega_z \ \text{ or } \ a_\perp \ll l_0 \ll a_z, \tag{1}$$

where $\omega_\perp$ (ω_z) is the trapping frequency in the radial (axial) direction, μ_g is the ground-state chemical potential, $a_\perp = [\hbar/(M\omega_\perp)]^{1/2}$ ($a_z = [\hbar/(M\omega_z)]^{1/2}$) is harmonic oscillator length in the radial (axial) direction, and $l_0 = \hbar/\sqrt{2M\mu_g}$ is healing length with M being mass of fermionic atom pair. In fact, in Q1D the motion of the condensate in the radial direction is frozen and governed by the ground-state wave function (i.e., zero-point oscillation) of the corresponding radial harmonic oscillator potential.[32] Notice that the Q1D condition [Eq. (1)] requires that the atomic number of the condensate must be very small (see Sec. III.A.2 of Ref. 32) and is hard to realize experimentally. In such system the dispersion term in the Bogoliubov excitation spectrum (i.e., k^3 term, with k being the wave number in axial direction) comes from the quantum pressure and hence has a positive coefficient, which results in the formation of dark solitons when a balance between interparticle interaction and quantum-pressure-induced dispersion is fulfilled. Up to now all superfluid Fermi gases in the BCS-BEC crossover realized experimentally, although being cigar-shaped, violate the Q1D condition [Eq. (1)]. It is easy to check that the system for measuring the sound propagation realized by Duke experimental group[28] is also a three-dimensional (3D) cigar-shaped condensate. The sound wave realized in that experiment is in fact a density perturbation of fermionic atom pairs consisting of propagating plane wave in the axial direction and a stationary distribution of Thomas-Fermi (TF) wave function in the radial direction. It is natural to ask the following question: is it possible to form a soliton in such cigar-shaped but 3D superfluid Fermi gas?

In this work we shall give a definite answer to the above question. We show that it is indeed available to generate a

soliton in a cigar-shaped, 3D superfluid Fermi gas even the Q1D condition is breakdown. However, the soliton obtained in this case is not a dark but bright one propagating on a continuous background of the condensate. Furthermore, different from the subsonic dark soliton obtained under Q1D condition[32] the bright soliton predicted here is supersonic one, i.e., its propagating velocity is larger than the linear sound speed. In addition, bright solitons in different superfluid regimes display different and interesting features, which may be used to characterize the different superfluid properties in different superfluid regimes of the BCS-BEC crossover. The formation of such supersonic bright soliton is due to the balance between interparticle interaction and a waveguidelike dispersion and hence a large particle number of the system is needed, which will be explained in detail below.

This paper is organized as follows. In Sec. II, we present superfluid hydrodynamics equations controlling the dynamics of a trapped superfluid Fermi gas, which are obtained from an equation of macroscopic wave function under TF approximation. In Sec. III we solve analytically the eigenvalue problem for linear collective excitations in a cigar-shaped 3D system by using a perturbation method and provide explicit results of all eigenvalues and eigenfunctions. The sound mode and its propagating velocity is discussed in detail and compared with the result of the Duke experiment. In Sec. IV we consider weak nonlinear excitations of the superfluid Fermi gas in the BCS-BEC crossover. We derive a Korteweg de Vries (KdV) equation by using a method of multiple scales and give supersonic bright soliton solutions. The physical features of the supersonic bright solitons in the BCS-BEC crossover are discussed and a numerical simulation for soliton evolution is also carried out. Finally, the last section contains a conclusion and discussion of our main results.

II. SUPERFLUID HYDRODYNAMIC EQUATIONS

We consider a superfluid Fermi gas, in which fermionic atoms (i.e., ^{6}Li or ^{40}K) have two different internal states with equal atomic number. In ground state all atoms are paired and condensed atom pair density is n_s. By means of Feshbach resonance technique the BCS-BEC crossover can be realized easily by tuning an applied magnetic field, and hence changing the s-wave scattering length a_s. Usually, a dimensionless interaction parameter $\eta \equiv 1/(k_F a_s)$ [$k_F = (6\pi^2 n_s)^{1/3}$ is Fermi wave number] is introduced to distinguish different superfluid regimes, i.e., BCS regime ($\eta \leq -1$), BEC regime ($\eta \geq 1$), and BEC-BCS crossover regime ($-1 < \eta < 1$). The special case $\eta = -\infty$ ($\eta = +\infty$) is called BCS (BEC) limit and $\eta = 0$ is called unitarity limit. Both theoretical and experimental studies show that the transition from BCS regime to BEC regime is smooth,[1] which means that the dynamical property of superfluid Fermi gases in various superfluid regimes can be investigated in a unified way.

Recently, an order-parameter (macroscopic wave function) equation controlling the dynamics of trapped superfluid Fermi gases in the BEC-BCS crossover at zero temperature is suggested,[15–22,30,32,33] which reads

$$i\hbar \frac{\partial \Psi_s}{\partial t} = \left[-\frac{\hbar^2 \nabla^2}{2M} + V_s(\mathbf{r}) + \mu_s(n_s) \right] \Psi_s, \tag{2}$$

where Ψ_s is the order parameter of condensed fermionic atomic pairs with the pair density $n_s = |\Psi_s|^2$ and the normalized condition $\int d\mathbf{r} |\Psi_s|^2 = N$ (N is the total atomic pair number of the superfluid Fermi gas), M is the mass of atom pair (i.e., $M = 2m$ with m being atomic mass), $V_s(\mathbf{r})$ is trapping potential, $\mu_s(n_s) = 2\mu(2n_s)$ with $\mu(n)$ being the bulk chemical potential (or called equation of state) which can be obtained under a local-density approximation and has the form $\mu(n) = \partial[n\varepsilon(n)]/\partial n$. Here $n = 2n_s$ is atomic density and $\varepsilon(n)$ is the bulk energy per particle obtained in the absence of the tapping potential. Introducing $\varepsilon(n) = (3/5)\varepsilon_F \sigma(\eta)$, with $\varepsilon_F = \hbar^2 k_F^2/(2m)$ being Fermi energy, one has $\mu(n) = \varepsilon_F[\sigma(\eta) - (\eta/5)\partial\sigma(\eta)/\partial\eta]$.[15–17,20,24,25] In general, the expression of $\mu(n)$ is very complicated but in many cases it can be approximated by the polytropic approximation[30,32]

$$\mu_s(n_s) = 2\mu^0 (n_s/n^0)^\gamma, \tag{3a}$$

$$\gamma = \gamma(\eta^0) = \left(\frac{n}{\mu} \frac{\partial\mu}{\partial n} \right)_{\eta=\eta^0}$$

$$= \frac{\frac{2}{3}\sigma(\eta^0) - \frac{2\eta^0}{5}\sigma'(\eta^0) + \frac{(\eta^0)^2}{15}\sigma''(\eta^0)}{\sigma(\eta^0) - \frac{\eta^0}{5}\sigma'(\eta^0)}, \tag{3b}$$

where μ^0 and n^0 are, respectively, reference chemical potential and particle-number density. Usually one takes n^0 to be the density of the ideal Fermi gas at the trapping center of the system. Thus one has $\mu^0 = \varepsilon_F^0[\sigma(\eta^0) - \eta^0\sigma'(\eta^0)/5]$ with $\varepsilon_F^0 = (\hbar k_F^0)^2/(2m)$, $\eta^0 = 1/(k_F^0 a_s)$, and $k_F^0 = (6\pi n^0)^{1/3}$. Notice that in the BEC limit (i.e., $\gamma = 1$) and under steady-state condition the order-parameter Eq. (2) reduces to the one derived by Pieri and Strinati[34] based on Bogoliubov de Gennes equations in an extended BCS theory.

Under the transformation $\Psi_s = \sqrt{n_s} \exp(i\frac{M}{\hbar}\int d\mathbf{r}\mathbf{v}_s)$, Eq. (2) converts into the superfluid hydrodynamic equations

$$\frac{\partial n_s}{\partial t} + \nabla \cdot (n_s \mathbf{v}_s) = 0, \tag{4a}$$

$$M\frac{\partial\mathbf{v}_s}{\partial t} + \nabla\left[\mu_s(n_s) + V_s(\mathbf{r}) + \frac{1}{2}M\mathbf{v}_s^2 - \frac{\hbar^2}{2M\sqrt{n_s}}\nabla^2\sqrt{n_s} \right] = 0, \tag{4b}$$

where $\mathbf{v}_s$ is superfluid velocity. The last term in the square bracket of Eq. (4b), i.e., $-\hbar^2\nabla^2\sqrt{n_s}/(2M\sqrt{n_s})$, is called quantum pressure. We know that the formation of soliton is due to an exact equilibrium between dispersion and nonlinear effects. In the case of Q1D, the dispersion is mainly provided by the quantum pressure and hence to form a soliton the quantum pressure must be taken into account. On the other hand, in Q1D the particle number of the condensate is very small and hence the quantum pressure is significant and thus cannot be neglected, which has been demonstrated clearly in the study of subsonic dark solitons in condensed bosonic

atomic gases with repulsive interaction[35–38] and in superfluid fermionic atomic gases.[32] The situation changes drastically if the atom-pair number N of the system is very large, which is the situation of nearly all experiments of ultracold Fermi gases up to now. Because $\mu_s(n_s)$ is always positive in the whole BCS-BEC crossover, for large N the quantum pressure effect plays a negligible role and thus can be neglected safely.[1,15–22,30,33] It seems that in this case a soliton cannot form because the dispersion contributed from the quantum pressure does not exist. However, for large N the Q1D condition is breakdown, the system becomes a 3D one and hence a new dispersion effect occurs. In fact, in the case of large N the ground-state wave function in radial direction is a TF type, which results in discrete eigenmodes of linear excitations in the radial direction, and hence induces a dispersion effect for the wave propagation in axial direction. So it is possible to use such "waveguide" dispersion to balance the nonlinearity contributed by the interparticle interaction [characterized by $\mu_s(n_s)$] to form a soliton in superfluid Fermi gases with large N, as shown below.

III. LINEAR COLLECTIVE EXCITATIONS AND SOUND SPEED

We now study linear collective excitations of the system. We assume the atom-pair number N is large, and hence ne-

glect the quantum pressure term in Eq. (4b). The ground-state solution of the superfluid hydrodynamic Eqs. (4a) and (4b) corresponds to $\partial/\partial t = 0$ and $\mathbf{v}_s = 0$, which yields

$$\mu_s[n_s^{\text{eq}}(\mathbf{r})] + V_s(\mathbf{r}) = \mu_g, \tag{5}$$

where μ_g is the ground-state chemical potential. Using the polytropic approximation [Eq. (3a)] we obtain $n_s^{\text{eq}}(\mathbf{r}) = n^0[\mu_g - V_s(\mathbf{r})]^{1/\gamma}/(2\mu^0)^{1/\gamma}$. As in most experiments we take the trapping potential with the form of axial symmetry

$$V_s(\mathbf{r}) = \frac{1}{2}M[\omega_\perp^2 r^2 + \omega_z^2 z^2], \tag{6}$$

where $r = \sqrt{x^2 + y^2}$ is radial coordinate. Thus we have

$$n_s^{\text{eq}}(\mathbf{r}) = n^0 \left(\frac{\mu_g}{2\mu^0}\right)^{1/\gamma} \left(1 - \frac{r^2}{R_\perp^2} - \frac{z^2}{R_z^2}\right)^{1/\gamma}, \tag{7}$$

where $R_\perp = (2\mu_g/M\omega_\perp^2)^{1/2}$ and $R_z = (2\mu_g/M\omega_z^2)^{1/2}$ are radial and axial half lengths of the condensate, respectively. We assume $\omega_z \ll \omega_\perp$ the condensate is hence a cigar-shaped one with the long axis along z direction. By the normalized condition $\int d\mathbf{r} n_s^{\text{eq}}(\mathbf{r}) = N$, it is easy to get the explicit expression of the chemical potential

$$\mu_g = 2\varepsilon_F^0 \left[\left(\frac{(\sigma(\eta^0) - \eta^0\sigma'(\eta^0))}{5}\right)^{1/\gamma} \frac{\pi^{1/2}(1+\gamma)\Gamma\left(\frac{1}{\gamma} + \frac{5}{2}\right)}{8\gamma\Gamma\left(\frac{1}{\gamma} + 2\right)}\right]^{2\gamma/2+3\gamma}. \tag{8}$$

When obtaining above result we have chosen the reference density n^0 as the value of a trapped but noninteracting Fermi gas, i.e., $n^0 = (2m\varepsilon_F^0)^{3/2}/(6\pi^2\hbar^3)$ (Refs. 28, 30, and 32) with $\varepsilon_F^0 = \hbar(6N\omega_\perp^2\omega_z)^{1/3}$.

Using the result of μ_g one can estimate the critical atom-pair number from 3D condensate to Q1D one. In fact, by the Q1D condition in Eq. (1) one obtains

$$N_{\text{1D}}^{\text{cr}} = \frac{\omega_\perp}{48\omega_z} \left[\left(\frac{(\sigma(\eta^0) - \eta^0\sigma'(\eta^0))}{5}\right)^{\frac{1}{\gamma}} \frac{\pi^{\frac{1}{2}}(1+\gamma)\Gamma\left(\frac{1}{\gamma} + \frac{5}{2}\right)}{8\gamma\Gamma\left(\frac{1}{\gamma} + 2\right)}\right]^{\frac{-6\gamma}{2+3\gamma}}, \tag{9}$$

i.e., if $N > N_{\text{1D}}^{\text{cr}}$ ($N < N_{\text{1D}}^{\text{cr}}$) the system is 3D (Q1D) condensate.[39] Using the formula (9) it is easy to check that $N \gg N_{\text{1D}}^{\text{cr}}$ in the Duke experiment[28] and hence the superfluid Fermi gas produced in Ref. 28 is not a Q1D but a 3D one.

Linear collective excitations are small perturbations to the ground state, whose equations can be obtained by taking $n_s(\mathbf{r}, t) = n_s^{\text{eq}}(\mathbf{r}) + [\delta n_s(\mathbf{r})\exp(-i\omega t) + \text{c.c.}]$ and $\mathbf{v}_s(\mathbf{r}, t) = \delta\mathbf{v}_s(\mathbf{r})\exp(-i\omega t) + \text{c.c.}$, where δn_s and $\delta\mathbf{v}_s$ are small quantities and ω is the oscillating frequency of the perturbations. Substituting them into the Eqs. (4a) and (4b) (with the quantum pressure term being neglected) one obtains the eigenvalue problem

$$-M\omega^2\delta n_s = \nabla \cdot \left\{n_s^{\text{eq}}(\mathbf{r})\nabla\left[\left(\frac{\partial\mu_s}{\partial n_s}\right)\bigg|_{n_s = n_s^{\text{eq}}(\mathbf{r})}\delta n_s\right]\right\}. \tag{10}$$

Since ω_z is much less than $\omega_\perp$, for obtaining an analytic result we disregard the axial part of the trapping potential (which will be included in the numerical simulation given later). Then the ground-state density is simplified into $n_s^{\text{eq}}(r) = n^0(\mu_g/2\mu^0)^{1/\gamma}(1 - r^2/R_\perp^2)^{1/\gamma}$. Taking $\delta n_s(\mathbf{r}) = \delta n_s(r, \varphi)\exp(ikz)$ (k is wave number in the axial direction), Eq. (10) is reduced into the dimensionless form

$$\bar{\nabla}_\perp \cdot \{(1-\bar{r}^2)^{1/\gamma}\bar{\nabla}_\perp[(1-\bar{r}^2)^{1-(1/\gamma)}\delta n_s(\bar{r},\varphi)]\} - \bar{k}^2(1-\bar{r}^2)\delta n_s(\bar{r},\varphi) = -\frac{2\bar{\omega}^2}{\gamma}\delta n_s(\bar{r},\varphi), \qquad (11)$$

where $\bar{\nabla}_\perp = [\partial/\partial\bar{r},(1/\bar{r})\partial/\partial\varphi]$, $\bar{r}=r/R_\perp$, $\bar{\omega}=\omega/\omega_\perp$, and $\bar{k}=kR_\perp$.

In order to solve above equation we introduce the following transformation:

$$\Psi(\bar{r},\varphi) = (1-\bar{r}^2)^{1-(1/\gamma)}\delta n_s(\bar{r},\varphi), \qquad (12)$$

then Eq. (11) is converted into the form

$$(\hat{H}_0 + \hat{H}')\Psi = Ew(\bar{r},\varphi)\Psi, \qquad (13)$$

where $E=-2\bar{\omega}^2/\gamma$ (eigenvalue), $w(\bar{r},\varphi)=(1-\bar{r}^2)^{(1/\gamma)-1}$ (weight function), $\hat{H}_0=\bar{\nabla}_\perp\cdot(1-\bar{r}^2)^{1/\gamma}\bar{\nabla}_\perp$, and $\hat{H}'=-\bar{k}^2(1-\bar{r}^2)^{1/\gamma}$. Notice that both $\hat{H}_0$ and $\hat{H}_1$ are Hermitian operators.

Solving the eigenvalue problem (13) for all k ($0<k<\infty$) exactly is not available. Ghosh and Machida[24] solved Eq. (11) by a numerical diagonalization, which was first used for condensed Bose gas (i.e., for the special case of $\gamma=1$) by Zaremba.[40] However, notice that for linear and nonlinear sound propagation problems we are interested in here, one needs only the result for small k. Thus we can solve Eq. (13) using the perturbation theory developed in quantum mechanics by taking $\hat{H}'$ as a perturbation Hamiltonian.

Assuming $\Psi_j=\Psi_j^{(0)}+\Psi_j^{(1)}+\Psi_j^{(2)}+\cdots$ and $E_j=E_j^{(0)}+E_j^{(1)}+E_j^{(2)}+\cdots$, where j is the index of eigenvalues and eigenfunctions, Eq. (13) becomes

$$\hat{H}_0\Psi_j^{(l)} - E_j^{(0)}w(\bar{r},\varphi)\Psi_j^{(l)} = S^{(l)}, \qquad (14)$$

($l=0,1,2,\ldots$), with $S^{(0)}=0$, $S^{(1)}=[E_j^{(1)}w(\bar{r},\varphi)-\hat{H}']\Psi_j^{(0)}$, $S^{(2)}=E_j^{(2)}w(\bar{r},\varphi)\Psi_j^{(0)}+[E_j^{(1)}w(\bar{r},\varphi)-\hat{H}']\Psi_j^{(1)}$, etc.

The zero-order ($l=0$) solution of Eq. (14) can be solved exactly.[24] The result reads

$$\Psi_{n_r m}^{(0)}(\bar{r},\varphi) = A_{n_r m}\bar{r}^{|m|}P_{n_r}^{[(1/\gamma)-1,|m|]}(2\bar{r}^2-1)e^{im\varphi}, \quad (15a)$$

$$E_{n_r m}^{(0)} = -\frac{2}{\gamma}\{|m|+2n_r[\gamma(n_r+|m|)+1]\}, \qquad (15b)$$

$$A_{n_r m}^2 = \frac{\Gamma(n_r+1)\Gamma\left(\dfrac{1}{\gamma}+n_r+|m|\right)\left(\dfrac{1}{\gamma}+2n_r+|m|\right)}{\pi\Gamma\left(n_r+\dfrac{1}{\gamma}\right)\Gamma(1+n_r+|m|)}, \qquad (15c)$$

where $P_n^{(a,b)}$ is a Jacob polynomial of order n, n_r, and m are radial and angular quantum numbers, respectively. It is easy to show the above eigenfunctions are orthogonal and normalized

$$\int_0^1\int_0^{2\pi}\bar{r}d\bar{r}d\varphi\,\Psi_{n_r'm'}^{(0)*}\Psi_{n_r m}^{(0)}w(\bar{r},\varphi) = \delta_{n_r n_r'}\delta_{mm'}. \qquad (16)$$

With the zero-order solution given above as an expansion basis for $\Psi_j^{(l)}$ [$j=(n_r,m)$] we can easily solve Eq. (14) for high-order approximations ($l=1,2,\ldots$). The first-order solution ($l=1$) is given by

$$E_j^{(1)} = H'_{jj}, \qquad (17a)$$

$$\Psi_j^{(1)} = \sum_{j'\neq j}\frac{H'_{j'j}}{E_j^{(0)}-E_{j'}^{(0)}}\Psi_{j'}^{(0)}, \qquad (17b)$$

where $H'_{j'j}=\langle\Psi_{j'}^{(0)}|\hat{H}'|\Psi_j^{(0)}\rangle \equiv \int_0^1\int_0^{2\pi}d\bar{r}d\varphi\bar{r}\Psi_{j'}^{(0)*}\hat{H}'\Psi_j^{(0)}$. The second-order solution ($l=2$) reads

$$E_j^{(2)} = -\sum_{l\neq j}\frac{|H'_{jl}|^2}{E_l^{(0)}-E_j^{(0)}}, \qquad (18a)$$

$$\Psi_j^{(2)} = \sum_{l'\neq j}\frac{1}{E_{l'}^{(0)}-E_j^{(0)}}\left(E_j^{(1)}A_{l'}-\sum_{l\neq j}A_l H'_{l'l}\right)\Psi_{l'}^{(0)}. \quad (18b)$$

All high-order approximation solutions can be obtained explicitly in a similar way, but it is not needed and thus omitted here.

Up to the second-order approximation the expressions of eigenvalues and eigenfunctions of Eq. (10) are given by

$$\omega_{n_r m}(\bar{k}) = \pm\,\omega_\perp\left[-\frac{\gamma}{2}(E_{n_r m}^{(0)}+E_{n_r m}^{(1)}+E_{n_r m}^{(2)})\right]^{1/2}, \quad (19)$$

$$\delta n_{s n_r m}(r,\varphi;\bar{k}) = \left(1-\frac{r^2}{R_\perp^2}\right)^{(1/\gamma)-1}(\Psi_{n_r m}^{(0)}+\Psi_{n_r m}^{(1)}+\Psi_{n_r m}^{(2)}), \qquad (20)$$

where $E_{n_r m}^{(l)}$ and $\Psi_{n_r m}^{(l)}$ are proportional to $\bar{k}^{2l}$.

In Table I we have listed the analytical expressions of eigenvalues up to the first three-order approximations for modes of axial symmetry (i.e., $m=0$ and $n_r=0,1,2,3$) with corresponding eigenfunctions given in Appendix A, which are calculated by using the analytical formulas (15a)–(15c), (16), (17a), (17b), (18a), and (18b). Shown in Fig. 1 are the

TABLE I. Expressions of eigenvalues of radial eigenmodes $(n_r,m)=(0,0)$, (1,0), (2,0), and (3,0). Here $A_{a,b,c,d,\ldots}\equiv a+b\gamma+c\gamma^2+d\gamma^3+\cdots$, $B_1\equiv A_{-5,-23,87,611,794,264}/(A_{1,5,6}A_{1,11,30}A_{1,3}^2A_{1,5}^2)$, and $B_2\equiv A_{-7,-61,153,2641,6634,4464}/(A_{1,9,20}A_{1,15,56}A_{1,5}^2A_{1,7}^2)$.

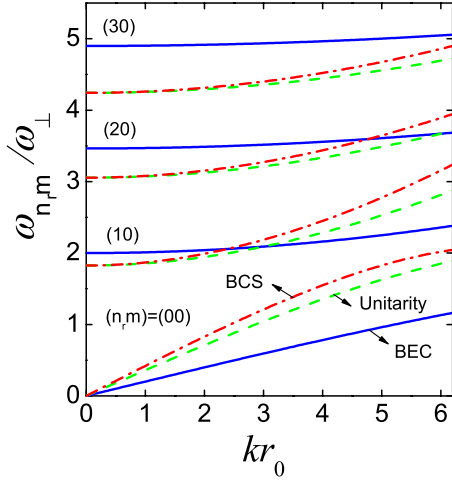|	(0,0)	(1,0)	(2,0)	(3,0)
$E_{n_r m}^{(0)}$	0	$-\dfrac{4A_{1,1}}{\gamma}$	$-\dfrac{8A_{1,2}}{\gamma}$	$-\dfrac{12A_{1,3}}{\gamma}$
$E_{n_r m}^{(1)}/\bar{k}^2$	$-\dfrac{1}{A_{1,1}}$	$-\dfrac{A_{1,1,2}}{A_{1,4,3}}$	$-\dfrac{A_{1,3,8}}{A_{1,8,15}}$	$-\dfrac{A_{1,5,18}}{A_{1,12,35}}$
$E_{n_r m}^{(2)}/\bar{k}^4$	$\dfrac{\gamma^3 A_{1,2}}{4A_{1,1}A_{1,3,2}^2}$	$-\dfrac{\gamma^3 A_{-3,-1,25,45,-2}}{4A_{1,1}^3 A_{1,3}^2 A_{1,7,12}}$	$-\dfrac{\gamma^3 B_1}{4}$	$-\dfrac{\gamma^3 B_2}{4}$

FIG. 1. (Color online) Multibranch spectrum of linear collective excitations for the modes of axial symmetry (i.e., $m=0$ and n_r $=0,1,2,3$) as functions of dimensionless parameter kr_0, with r_0 $=[2\varepsilon_F^0/(M\omega_\perp^2)]^{1/2}$. Solid, dashed, and dash-dotted lines correspond to $\eta^0 \equiv 1/(k_F^0 a_s)=5$ (near BEC limit), $\eta^0=0$ (unitarity limit), and $\eta^0=-1$ (BCS regime), respectively.

dimensionless eigenfrequencies (multibranch spectrum) $\omega_{n_r m}/\omega_\perp$ for these modes as functions of dimensionless wave number kr_0, with $r_0=[2\varepsilon_F^0/(M\omega_\perp^2)]^{1/2}$. In the figure, solid, dashed, and dash-dotted lines correspond to $\eta^0 \equiv 1/(k_F^0 a_s)$ $=5$ (near BEC limit), $\eta^0=0$ (unitarity limit), and $\eta^0=-1$

(BCS regime), respectively. Note that the dimensionless wave number $\bar{k}=kR_\perp$ in the expressions of the eigenfrequencies in Table I is normalized by the radius of the condensate. However, for the comparison of the eigenfrequencies in different superfluid regimes, $kR_\perp$ is not good variable because it varies along the BCS-BEC crossover for the same k. Thus in Fig. 1 we plot the eigenfrequencies as functions of kr_0, where $r_0=[2\varepsilon_F^0/(M\omega_\perp^2)]^{1/2}$ is a fixed number for given atom-pair number N, and the trapping frequencies $\omega_\perp$ and ω_z. From the figure we see that in different superfluid regimes the eigenfrequencies display different behavior. For (n_r,m) $=(0,0)$ mode, for a given k the eigenfrequency of the BCS regime is larger than that of the unitarity regime. In the BEC regime, the eigenfrequency is lowest. However, for $n_r \neq 0$, this property changes, which can be clearly seen from the figure. For the $(n_r,m)=(3,0)$ mode, the eigenfrequency of the BEC regime becomes largest. Such features of oscillatory frequencies of eigencollective excitations have also be found by Ghosh and Machida[24] in their numerical approach, but our result is an analytical one.

In Fig. 2 we have plotted the eigenfunctions of collective excitations $\delta n_{sn_r m}(r,\varphi)$ as functions of $\bar{r}=r/R_\perp$, given by Eq. (20). Notice that under TF approximation, the particle density in the radial boundary should be vanishing (i.e., $n_s|_{r=R_\perp}=0$), which requires $\delta n_s|_{r=R_\perp}=0$. For $\gamma<1$, all eigenfunctions obtained above possess this property. However, in the BEC limit (i.e., $\gamma=1$) a difficulty occurs at $r=R_\perp$ because δn_s is proportional to $(1-r^2/R_\perp^2)^{1/\gamma-1}$, see Eq. (20). This dif-
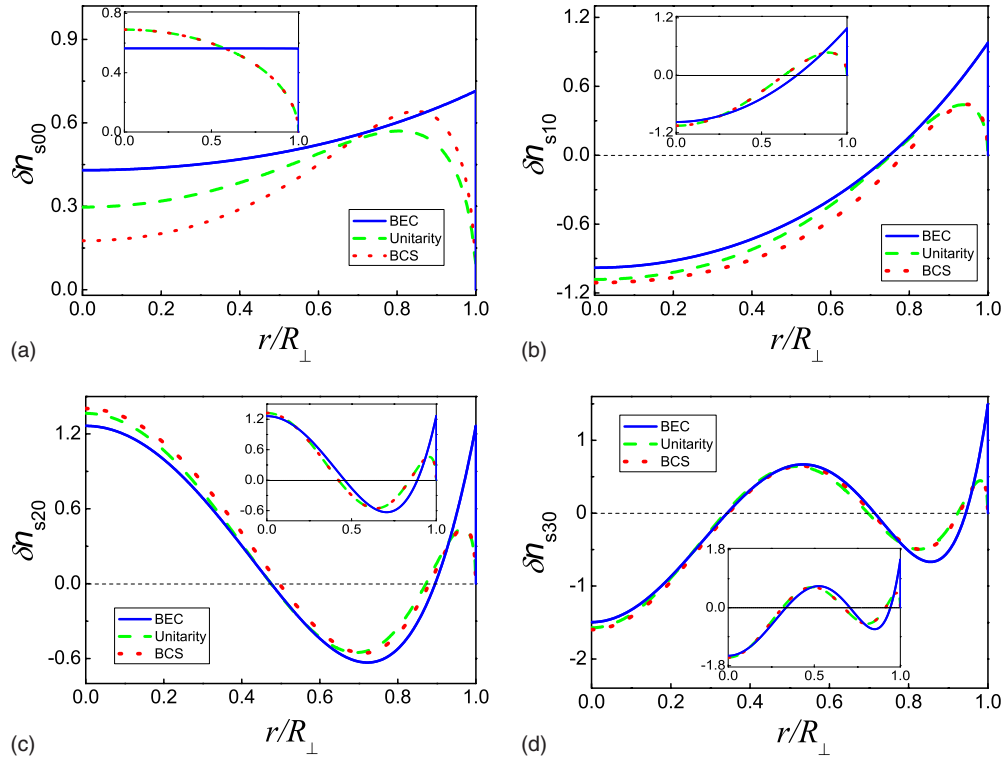

FIG. 2. (Color online) Eigenfunctions of collective excitations of the trapped Fermi superfluid. Panels (a), (b), (c), and (d) are, respectively, for modes $(n_r,m)=(0,0),(1,0),(2,0)$, and $(3,0)$ as a function of $r/R_\perp$. Solid, dashed, and dotted lines are for to $\eta^0 \equiv 1/(k_F^0 a_s)=5$ (near BEC limit), $\eta^0=0$ (unitarity limit), and $\eta^0=-1$ (BCS regime), respectively. In all panels the dimensional wave number $\bar{k}=5$ is selected, and insets are corresponding eigenfunctions for $\bar{k}=0$.

ficulty may be solved by understanding the BEC limit as $\gamma = 1 - \varepsilon$ (with ε a very small positive number) and $\delta n_s|_{r=R_\perp} \equiv \lim_{\varepsilon \to 0} \lim_{r \to R_\perp} \delta n_s = 0$.

Panels (a), (b), (c), and (d) of Fig. 2 are for $(n_r, m) = (0,0)$, $(1,0)$, $(2,0)$, and $(3,0)$ modes, respectively. In each panel, the solid, dashed, and dotted lines are, respectively, for $\eta^0 \equiv 1/(k_F^0 a_s) = 5$ (near BEC limit), $\eta^0 = 0$ (unitarity limit), and $\eta^0 = -1$ (BCS regime). In all panels the dimensional wave number $\bar{k} = 5$ is chosen, and insets are corresponding eigenfunctions for $\bar{k} = 0$. Notice that for the near BEC case δn_s has very large value at the radial boundary of the condensate, but it decreases rapidly (but smoothly) to zero near $r = R_\perp$. The peak of δn_s appeared at $r = R_\perp$ is due to the problem of figure resolution. In fact, δn_s is smooth near $r = R_\perp$ if using a small scaling for r. As expected, with an increase in n_r the number of radial nodes of the eigenfunction increases. For large n_r, the eigenfunction has a significant oscillation with respect to $r/R_\perp$. So in principle, for higher-order eigenmodes the TF approximation will be violated. However, our main focus here is on the low-lying collective modes and hence the TF approximation is valid.

We now discuss the sound propagation of the system, which corresponds to the lowest branch $\omega_{00}(k)$ of Fig. 1 that satisfies $\omega_{00}(0) = 0$ (Bogoliubov spectrum). By Eq. (19) with $(n_r, m) = (0,0)$ we obtain

$$\frac{\omega_{00}(\bar{k})}{\omega_\perp} = \pm \left(\frac{\gamma}{2(\gamma+1)} \right)^{1/2} \left[1 - \frac{\gamma^3(2\gamma+1)\bar{k}^2}{4(1+3\gamma+2\gamma^2)^2} \right]^{1/2} \bar{k}. \tag{21}$$

For small wave number $\omega_{00}(\bar{k})$ is proportional to $\bar{k}$. So we have $\omega_{00} = \pm ck$, with

$$c = \sqrt{\frac{\gamma \mu_g}{(1+\gamma)M}}, \tag{22}$$

being the sound speed of the system, where μ_g is given by Eq. (8). The "+" and "−" signs in Eq. (21) means that generally the sound wave can propagate in two different directions. The solid line of Fig. 3 is the result of the sound speed [in unit of Fermi velocity $v_F = (2\varepsilon_F^0/m)^{1/2}$] of the superfluid ^{6}Li atomic gas as a function of $\eta^0 = 1/(k_F^0 a_s)$, calculated by using the experimental parameters of Joseph *et al.*,[28] i.e., $N = 3 \times 10^5$, $\omega_\perp = 2\pi \times 688$ Hz, $\omega_z = 2\pi \times 34.4$ Hz. Thus one has $\varepsilon_F = \hbar^2(k_F^0)^2/2m = \hbar(6N\omega_\perp^2\omega_z)^{1/3} = k_B \times 1.4 \ \mu K$ (k_B is Boltzmann's constant), and hence $1/k_F^0 = 0.17 \ \mu m$, and $n^0 = (k_F^0)^3/(6\pi^2) = 4 \times 10^{12} \ cm^{-3}$. The experimental data measured by Joseph *et al.*[28] are denoted by open squares. We see that our theoretical result agrees quite well with that of Joseph *et al.*[28] For comparison, in Fig. 3 we have also plotted the result of the sound speed of the Q1D superfluid Fermi gas,[32] which is given by the dashed line. One sees that the Q1D sound speed is obviously lower than the 3D one. The reason is that in the Q1D system there is a very strong confinement in radial direction, which results in a decrease in sound speed.
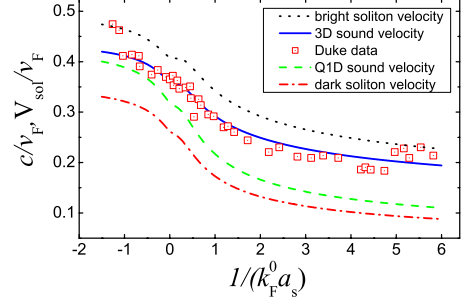

FIG. 3. (Color online) The sound speed c of the cigar-shaped but 3D superfluid gas ^{6}Li atomic gas as a function of $\eta^0 = 1/(k_F^0 a_s)$. The solid line is the theoretical result by using Eq. (22), whereas the open squares are the data measured by the Duke experiment Joseph (Ref. 28). For comparison, in the figure we have also plotted the sound speed of Q1D case (dashed line), the propagating velocity V_{sol} of the subsonic dark soliton in Q1D (dotted-dashed line), and the supersonic bright soliton in the present 3D case (the dotted line). All velocities are in unit of corresponding Fermi velocity of $v_F = (2\varepsilon_F^0/m)^{1/2}$.

IV. WEAK NONLINEAR EXCITATIONS AND BRIGHT SOLITONS

We now turn to investigate large-amplitude sound wave of the system. From the expression of eigenvalues in Eq. (19) we see that each eigenmode has dispersion. On the other hand, there is nonlinearity contributed by interparticle interaction, characterizing by $\mu_s(n_s)$ in the hydrodynamic Eq. (4b). Thus one expects possible soliton formation in the system via the balance between the dispersion and nonlinearity. In the case of large N, the superfluid velocity $\mathbf{v}_s = (v_r, v_\varphi, v_z)$ satisfy hydrodynamic Eqs. (4a) and (4b), which in cylindrical coordinate system can be written as the form

$$\frac{\partial n_s}{\partial t} + \frac{1}{r}\frac{\partial}{\partial r}(rn_s v_r) + \frac{1}{r}\frac{\partial}{\partial \varphi}(n_s v_\varphi) + \frac{\partial}{\partial z}(n_s v_z) = 0, \tag{23a}$$

$$M\frac{\partial v_\varphi}{\partial t} + \frac{1}{r}\frac{\partial}{\partial \varphi}\left[\frac{1}{2}M(v_r^2 + v_\varphi^2 + v_z^2) + \mu_s(n_s) + V_s(r,z) \right] = 0, \tag{23b}$$

$$M\frac{\partial v_r}{\partial t} + \frac{\partial}{\partial r}\left[\frac{1}{2}M(v_r^2 + v_\varphi^2 + v_z^2) + \mu_s(n_s) + V_s(r,z) \right] = 0, \tag{23c}$$

$$M\frac{\partial v_z}{\partial t} + \frac{\partial}{\partial z}\left[\frac{1}{2}M(v_r^2 + v_\varphi^2 + v_z^2) + \mu_s(n_s) + V_s(r,z) \right] = 0, \tag{23d}$$

where $V_s(r,z)$ is given by Eq. (6). For simplicity we focus our effort here to a cylindrically symmetric excitation. In this case, one has $\partial/\partial\varphi = 0$ and $v_\varphi = 0$. For a weak nonlinear sound wave, its linear correspondence is the mode $(n_r, m) = (0,0)$ with vanishing wave number k. Since the dynamics of the system can be characterized by two different time scales, i.e., the fast motion in the radial direction and the slow motion in the axial direction. In order to make an ana-

lytical approach available, we assume the trapping potential is z independent, i.e., $V_s(r,z) = V_s(r)$. The effect of axial inhomogeneity will be considered in later numerical simulation. Introducing the slow variables $\xi = \epsilon(z - ct)$ and $\tau = \epsilon^3 t$, where ϵ is a small parameter representing the relative amplitude of the excitation and c is an undetermined parameter, and making the asymptotic expansions $n_s = n_s^{eq} + \epsilon^2 n^{(0)} + \epsilon^4 n^{(1)} + \cdots$, $v_r = \epsilon^3 u^{(0)} + \epsilon^5 u^{(1)} + \cdots$, $v_z = \epsilon^2 w^{(0)} + \epsilon^4 w^{(1)} + \cdots$, Eqs. (23a)–(23d) become

$$-c\frac{\partial}{\partial\xi}n^{(l)} + \frac{1}{r}\frac{\partial}{\partial r}[rn_s^{eq}u^{(l)}] + \frac{\partial}{\partial\xi}[n_s^{eq}w^{(l)}] = \alpha^{(l)}, \quad (24a)$$

$$\frac{\partial}{\partial r}[\mu_s' n^{(l)}] = \beta^{(l)}, \quad (24b)$$

$$-Mc\frac{\partial}{\partial\xi}w^{(l)} + \frac{\partial}{\partial\xi}[\mu_s' n^{(l)}] = \gamma^{(l)}, \quad (24c)$$

where $\mu_s' \equiv \partial\mu_s(n_s)/\partial n_s|_{n_s = n_s^{eq}}$. Explicit expressions of $\alpha^{(l)}$, $\beta^{(l)}$, and $\gamma^{(l)}$ $(l = 0, 1, \ldots)$ are presented in Appendix B. For convenience, we convert Eq. (24) into the following form:

$$\mu_s' n^{(l)} = [\mu_s' n^{(l)}]|_{r=0} + \int_0^r dr\beta^{(l)}, \quad (25a)$$

$$\frac{1}{r}\frac{\partial}{\partial r}[rn_s^{eq}u^{(l)}] = \alpha^{(l)} + \left(c - \frac{n_s^{eq}\mu_s'}{Mc}\right)\frac{\partial n^{(l)}}{\partial\xi} + \frac{n_s^{eq}\gamma^{(l)}}{Mc}, \quad (25b)$$

$$w^{(l)} = \int d\xi \frac{1}{Mc}\left[\mu_s'\frac{\partial n^{(l)}}{\partial\xi} - \gamma^{(l)}\right]. \quad (25c)$$

Eqs. (25a)–(25c) can be solved order by order. At the lowest order ($l = 0$), from Eq. (25a) we obtain

$$n^{(0)}(r,\xi,\tau) = \frac{\mu_s'|_{r=0}}{\mu_s'}F(\xi,\tau), \quad (26)$$

where $F(\xi,\tau) = n^{(0)}(0,\xi,\tau)$ is an envelope function to be determined yet. Notice that $\mu_s'|_{r=0}/\mu_s' = (1 - r^2/R_\perp^2)^{1/\gamma - 1}$ corresponds to the leading-order approximation of Eq. (17b) for the $(n_r, m) = (0,0)$ eigenmode. By Eq. (25c) we have

$$w^{(0)} = \frac{\mu_s'|_{r=0}}{Mc}F(\xi,\tau). \quad (27)$$

Integrating Eq. (25b) (for $l = 0$) from 0 to r, we obtain

$$rn_s^{eq}u^{(0)} = \mu_s'|_{r=0}\frac{\partial F}{\partial\xi}\int_0^r dr\left[\frac{cr}{\mu_s'} - \frac{rn_s^{eq}}{Mc}\right]. \quad (28)$$

Because $n_s^{eq}|_{r=R_\perp} = 0$, by Eq. (28) we obtain $\int_0^{R_\perp} dr[cr/\mu_s' - rn_s^{eq}/(Mc)] = 0$, which yields the sound speed

$$c^2 = \frac{\int_0^{R_\perp} dr r n_s^{eq}}{M\int_0^{R_\perp} dr r/\mu_s'} = \frac{\gamma\mu_g}{M(1 + \gamma)}. \quad (29)$$

This result agrees exactly with that obtained by Capuzzi *et al.*[25] by using a different approach.[41] The second equality agrees also with that obtained by the linear theory of collective excitations developed in Sec. III [see Eq. (22)].

Notice that the sound-speed formula for the same system was also studied in Ref. 24. However, the result in that work is incorrect because of the use of incorrect orthonality condition of eigenfunctions of linear excitations, which was pointed out by the authors of Ref. 42. We also note that the first sound and second sound of a superfluid Fermi gas has been discussed in Ref. 27 by using a two-fluid model. However, the trapping potential they used is a spherical symmetric one and the system works at finite temperature. Hence, the sound speed they obtained is different from that obtained in our system, which is valid for zero temperature and for an axially symmetric trap.

Generally, Eq. (28) gives the expression of $u^{(0)}$

$$u^{(0)} = -\frac{\gamma rc}{2F_0}\frac{\partial F}{\partial\xi}, \quad (30)$$

where $F_0 = n^0(\mu_g/2\mu^0)^{1/\gamma}$ is central number density in the ground state.

Using above leading-order solution we go to the next order. Equation (25b) for $l = 1$ reads

$$\frac{\partial}{\partial r}[rn_s^{eq}u^{(1)}] = -rJ_0(r)\frac{\partial F}{\partial\tau} - rJ_1(r)\frac{\partial^3 F}{\partial\xi^3} - rJ_2(r)F\frac{\partial F}{\partial\xi} \quad (31)$$

with

$$J_0(r) = \left(1 - \frac{r^2}{R_\perp^2}\right)^{(1/\gamma)-1}\left[2 + \gamma - (\gamma+1)\frac{r^2}{R_\perp^2}\right], \quad (32a)$$

$$J_1(r) = -\frac{\gamma c r^2}{4(1+\gamma)}\left(1 - \frac{r^2}{R_\perp^2}\right)^{(1/\gamma)-1}\left[\gamma - (\gamma+1)\frac{r^2}{R_\perp^2}\right], \quad (32b)$$

$$J_2(r) = \frac{c}{F_0}\left(1 - \frac{r^2}{R_\perp^2}\right)^{(1/\gamma)-2}\left[2\gamma^2 + 3\gamma + 2 - (4\gamma^4 + 5\gamma + 2)\frac{r^2}{R_\perp^2} + 2\gamma(\gamma+1)\frac{r^4}{R_\perp^4}\right]. \quad (32c)$$

Integrating Eq. (31) from 0 to $R_\perp$, we obtain the equation for the envelope function $F(\xi,\tau)$

$$\frac{\partial F}{\partial\tau} + \lambda_1 F\frac{\partial F}{\partial\xi} + \lambda_2\frac{\partial^3 F}{\partial\xi^3} = 0 \quad (33)$$

with $\lambda_1 = c(3\gamma + 2)/(2F_0)$ and $\lambda_2 = \gamma^3 R_\perp^2 c/[8(1+\gamma)(1+3\gamma+2\gamma^2)]$.

Letting $G = \epsilon^2 F$ and using the definitions of $\xi = \epsilon Z$ and $\tau = \epsilon^3 t$, we have

$$\frac{\partial G}{\partial t} + \lambda_1 G \frac{\partial G}{\partial Z} + \lambda_2 \frac{\partial^3 G}{\partial Z^3} = 0 \qquad (34)$$

with $Z = z - ct$. Equation (34) is well-known KdV equation, a completely integrable system and admits multisoliton solutions. A single soliton solution is given by

$$G = A_0 \, \text{sech}^2\left(\frac{z - V_{\text{sol}}t - z_0}{\sigma}\right) \qquad (35)$$

with

$$V_{\text{sol}} = c\left(1 + \frac{3\gamma + 2}{6}\frac{A_0}{F_0}\right), \qquad (36a)$$

$$\sigma = R_\perp \left[\frac{3\gamma^3 F_0}{(1 + \gamma)(1 + 3\gamma + 2\gamma^2)(3\gamma + 2)A_0}\right]^{1/2}, \quad (36b)$$

where A_0 is a positive constant and z_0 is an arbitrary real constant depending on initial exciting condition.

Based on above results we obtain

$$n_s = F_0\left(1 - \frac{r^2}{R_\perp^2}\right)^{1/\gamma}$$
$$+ \left(1 - \frac{r^2}{R_\perp^2}\right)^{(1/\gamma)-1} A_0 \, \text{sech}^2\left(\frac{z - V_{\text{sol}}t - z_0}{\sigma}\right), \quad (37a)$$

$$v_z = \frac{(1 + \gamma)cA_0}{F_0} \text{sech}^2\left(\frac{z - V_{\text{sol}}t - z_0}{\sigma}\right), \qquad (37b)$$

$$v_r = \frac{\gamma cA_0}{\sigma F_0} r \, \text{sech}^2\left(\frac{z - V_{\text{sol}}t - z_0}{\sigma}\right)\tanh\left(\frac{z - V_{\text{sol}}t - z_0}{\sigma}\right), \qquad (37c)$$

when exact to the leading-order approximation. We see that the soliton obtained is indeed a bright one that propagates on a condensate background. This is quite different from the result in Q1D case where the soliton obtained is a dark one.[32] In addition, from Eq. (36a) we see that the bright soliton is supersonic because its propagating velocity is larger than the sound speed c, which is also different from the dark soliton in Q1D case where the soliton obtained is a subsonic one.[32]

The physical reason for the occurrence of the bright soliton can be understood as follows. From the Bogoliubov spectrum in Eq. (21) we know that the coefficient of k^3 (when making an expansion around $k = 0$) is negative, which is different from that obtained for Q1D case where the coefficient of k^3 is positive.[32] The difference between the sign of the k^3 coefficient for the present 3D system and that of the Q1D system studied in Ref. 32 is due to the different origin of dispersion. In the Q1D case the dispersion mainly comes from quantum pressure, whereas in the present 3D case the dispersion results from the TF distribution of ground-state wave function in the radial direction, which induces a dispersion for each eigenmode. One can make a simple comparison between the propagation of collective excitations in

the present cigar-shaped condensate and the light propagation in optical fibers. The dispersion induced by the quantum pressure is analogy to a "material dispersion," while the dispersion originated by the TF ground-state distribution is analogy to "waveguide dispersion."[43] It is just due to these different dispersion characters that make subsonic dark solitons occur in the Q1D system[32] but the supersonic bright solitons possible in the present 3D system.

In order to give a quantitative picture for the feature of the bright soliton predicted above, in Table II we have we presented some numerical values of velocity V_{sol}, width σ of the bright soliton in terms of Duke experimental parameters.[28] The condensate radii $R_\perp$ and R_z are also given. We see that the bright soliton has different velocity and width in different superfluid regimes. When passing from the BEC to the BCS regimes, the propagating velocity and axial width of the soliton increases. This is contrast to the Q1D dark solitons, for which the soliton width in the BCS regime is smaller than that in the BEC regime.

For comparison, in Fig. 3 we have plotted the propagating velocity of the bright soliton for the present 3D system (the dotted line), and that of the dark soliton for the Q1D system given in Ref. 32 (dotted-dashed line). We see clearly that the former is supersonic and the latter is subsonic. We note that both the sound speed and soliton velocity display a discontinuous derivative at $\eta^0 = 0$. This is an artifact resulted from the analytical fitting formula for the equation of state proposed by Manini and Salasnich (see Fig. 1 in Ref. 16) that has a discontinuous derivation at $\eta^0 = 0$. Of course, there should be no discontinuous derivative for them because the crossover from BCS to BEC is smooth.

Now we address the stability problem of the supersonic bright solitons in ultracold Fermi gases. Because the KdV Eq. (33) is a completely integrable mathematical model,[44] its soliton solutions are stable to external 1D perturbations. Notice that when obtaining the KdV Eq. (33) we have assumed weak dispersion and weak nonlinear conditions. In addition, the axial trapping potential, i.e., $M\omega_z^2 z^2/2$ in the Eqs. (23b)–(23d), has been disregarded. However, this may be not the realistic case of ultracold Fermi gas experiments, where for large-amplitude and narrow-width collective excitations and for a long propagating distance, effects originated from high-order dispersion, high-order nonlinearity, and axial inhomogeneity may play significant role, and hence (these structural perturbations) will destroy the integrability of the KdV equation. For weak dispersive and weak nonlinear excitations we discussed here, the instability of solitons is
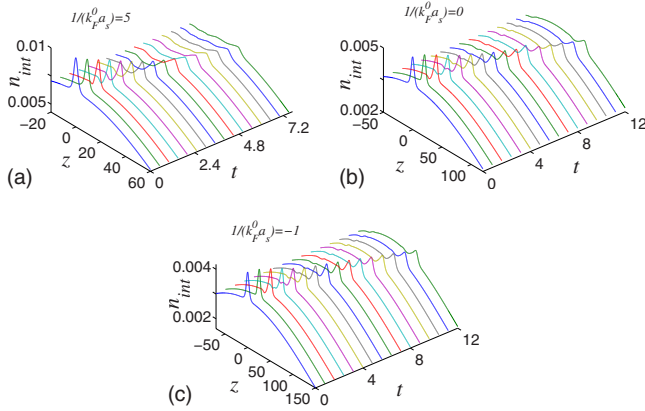
TABLE II. Numerical values of the bright soliton velocity V_{sol}, axial width σ, and condensate radii $R_\perp$ and R_z for $A_0/F_0 = 0.1$ in several different superfluid regimes.

	BEC limit	BEC regime	Unitarity	BCS regime
$\eta^0 = 1/(k_F^0 a_s)$	5	1	0	−1
V_{sol} (mm/s)	12	17	20	24
σ (μm)	3.5	5	6	6.5
$2R_z$ (μm)	198	284	397	467
$R_\perp$ (μm)	5	7	10	12

FIG. 4. (Color online) Result of numerical simulation on the evolution of bright soliton as a function of dimensionless time t (in unit of 0.05 ms) and axial distance z (in unit of 0.5 μm). The vertical coordinate is the integrated density $n_{int}(z)$ $=2\pi\int_0^R dr n_s(r,z)$. Panels (a), (b), and (c) correspond to the BEC regime $[1/(k_F^0 a_s)=5]$, unitarity limit $1/(k_F^0 a_s)=0$, and BCS regime $[1/(k_F^0 a_s)=-1]$, respectively.

mainly due to the axial inhomogeneity contributed by the axial trapping potential. An analytical study of the instability (including its deformation, radiation, and even disintegration) of the supersonic bight soliton can be done by using a similar method developed in Ref. 36, which is, however, a topic beyond scope of the present work and will be published elsewhere.[45] To show the influence of the axial trapping potential on the supersonic bright soliton predicted above, here we make a numerical simulation starting from the hydrodynamics Eqs. (23a)–(23d) by using the bright soliton solution in Eq. (37) as an initial condition. The system parameters are chosen as $N=1\times10^5$, $\omega_\perp=2\pi\times3000$ Hz, $\omega_z=2\pi\times100$ Hz, and $A_0/F_0=0.2$. The result of the simulation for three different regimes are illustrated in Fig. 4. Panels (a), (b), and (c) in the figure correspond to bright soliton propagation in the BEC $[1/(k_F^0 a_s)=5]$, unitarity limit $[1/(k_F^0 a_s)=0]$, and BCS $[1/(k_F^0 a_s)=-1]$ regimes, respectively. One can observe the following propagation features. (i) The bright soliton is fairly stable near the center of the condensate, but it becomes broadened and radiates small continuous waves when moving to the boundary of the condensate. This effect contributes mainly from the weak axial trapping potential that confines the condensate in the axial direction, not considered in the theoretical analysis given above. (ii) The soliton in the BCS regime is more stable than in the BEC regime. The reason is that, for the same N, $\omega_\perp$, and ω_z the axial length of the condensate in the BCS regime is much larger than that in the BEC regime, and hence the axial trapping potential plays less important role than in the BCS regime. (iii) During propagation, the bright soliton radiates a small dip that propagates in opposite direction. This phenomenon can be understood as follows. Because the hydrodynamics Eqs. (23a)–(23d) allow two eigensound-wave modes, one propagates with velocity c and another one propagates with velocity $-c$ [see Eq. (21) for small $\bar{k}$]. Thus an initial disturbance of the system Eqs. (23a)–(23d), though being a soliton solution of the KdV Eq. (33), will generally evolve into two

parts that having opposite propagating directions. (iv) In different superfluid regimes the supersonic bright soliton and associated radiation has different amplitude and propagating velocity. This is a direct reflection of different physical properties of the superfluid Fermi gas that can be used to distinguish different superfluid regimes of the system.

V. DISCUSSION AND SUMMARY

We have studied the linear and nonlinear sound propagation in a cigar-shaped, 3D superfluid Fermi gas with large particle number. We have solved analytically the eigenvalue problem of linear collective excitations by means of a perturbation method and provided explicit expressions of all eigenvalues and eigenfunctions. The results obtained are valid for all superfluid regimes in the BCS-BEC crossover. Based on these results we have discussed the sound propagation in the system and showed that the sound speed obtained in our calculation agrees well with experimental measurement by Joseph et al.[28] In addition, we have investigated the nonlinear sound propagation in the system and showed that the amplitude of excitations satisfies a KdV equation. Different from the result obtained in the Q1D case studied in Ref. 32, where subsonic dark solitons are obtained via the balance between quantum pressure and interparticle interaction, we have demonstrated that bright solitons with supersonic propagating velocity can be generated in the present 3D superfluid Fermi gas in the BCS-BEC crossover through the balance between a waveguidelike dispersion and the interparticle interaction.

We note that Jackson et al.[46] have studied solitons in atomic clouds of BEC limit. However, their result is valid for the case of small particle number, and hence the dark soliton obtained have Q1D characters. For large particle number, the confinement-induced dispersion (which has not been considered by Jackson et al.[46]) should be taken into account, as demonstrated in our present work. If increasing particle number from small to large, the system may display a crossover from 1D to 3D, and hence a transition from dark soliton to bright soliton may occur, an interesting topic that deserves to be studied in detail.

Experimentally, the supersonic bright solitons predicted here can be generated by using the method similar to that used to produce sound waves.[28,47] To produce a large and positive (bright) density perturbation, a focused and blueshifted laser beam should be switched on suddenly.[47] This method may generate two positive density pulses that propagate in opposite directions, and hence can be used to study the interaction between two bright solitons. The theoretical results presented here may be useful for understanding the nonlinear property of fermionic condensates and guiding experimental findings of the various nonlinear excitations in superfluid Fermi atomic gases in the BCS-BEC crossover.

APPENDIX A: EXPRESSIONS FOR EIGENFUNCTIONS DISCRETE MODES

The eigenfunctions of Eq. (13) up to second-order approximation are given by $\Psi_{n,m} = \Psi_{n,m}^{(0)} + \Psi_{n,m}^{(1)} + \Psi_{n,m}^{(2)}$, with $\Psi_{n,m}^{(1)}$ and $\Psi_{n,m}^{(2)}$ being first-order and second-order corrections, respectively. Defining $A_{a,b,c,d,\ldots}^q = (a + b\gamma + c\gamma^2 + d\gamma^3 + \cdots)^q$ and $\Psi_n^{(0)} = \Psi_{n0}^{(0)}$, we obtain

(1) The mode $(n_r, m) = (0,0)$

$$\Psi_0^{(0)} = \sqrt{\frac{1}{\gamma\pi}}, \tag{A1a}$$

$$\Psi_0^{(1)}/\bar{k}^2 = \frac{\gamma^2 A_{1,2}^{1/2}}{4 A_{1,1} A_{1,3,2}} \Psi_1^{(0)}, \tag{A1b}$$

$$\Psi_0^{(2)}/\bar{k}^4 = \frac{\gamma^4 A_{1,-1}}{8 A_{1,2}^{1/2} A_{1,1}^3 A_{1,4,3}} \Psi_1^{(0)} + \frac{\gamma^4 A_{1,4}^{1/2}}{16 A_{1,3,2} A_{1,9,26,24}} \Psi_2^{(0)}. \tag{A1c}$$

(2) The mode (1,0)

$$\Psi_1^{(0)} = -\sqrt{\frac{A_{1,2}}{\gamma\pi}}\left(1 - \frac{A_{1,1}}{\gamma}\bar{r}^2\right), \tag{A2a}$$

$$\Psi_1^{(1)}/\bar{k}^2 = -\frac{\gamma^2 A_{1,2}^{1/2}}{4 A_{1,1} A_{1,3,2}} \Psi_0^{(0)} + \frac{\gamma^2 A_{1,2}^{1/2} A_{1,4}^{1/2} A_{1,1}}{2 A_{1,3} A_{1,9,26,24}} \Psi_2^{(0)}, \tag{A2b}$$

$$\Psi_1^{(2)}/\bar{k}^4 = \frac{\gamma^4 A_{-1,1}}{8 A_{1,2}^{1/2} A_{1,4,3} A_{1,1}^3} \Psi_0^{(0)} + \frac{\gamma^4 A_{1,2}^{1/2} A_{1,4}^{1/2} A_{1,-2,1}}{4 A_{1,8,15} A_{1,9,26,24} A_{1,3}^2} \Psi_2^{(0)} + \frac{3\gamma^4 A_{1,2}^{1/2} A_{1,6}^{1/2} A_{1,1}}{16 A_{1,4} A_{1,15,74,120} A_{1,3}^2} \Psi_3^{(0)}. \tag{A2c}$$

(3) The mode (2,0)

$$\Psi_2^{(0)} = \sqrt{\frac{A_{1,4}}{\gamma\pi}}\left(1 - \frac{2A_{1,2}}{\gamma}\bar{r}^2 + \frac{A_{1,2} A_{1,3}}{2\gamma^2}\bar{r}^4\right), \tag{A3a}$$

$$\Psi_2^{(1)}/\bar{k}^2 = -\frac{\gamma^2 A_{1,2}^{1/2} A_{1,4}^{1/2} A_{1,1}}{2 A_{1,3} A_{1,9,26,24}} \Psi_1^{(0)} + \frac{3\gamma^2 A_{1,4}^{1/2} A_{1,6}^{1/2} A_{1,2}}{4 A_{1,5} A_{1,15,74,120}} \Psi_3^{(0)} \tag{A3b}$$

$$\Psi_2^{(2)}/\bar{k}^4 = \frac{\gamma^4 A_{1,4}^{1/2}}{16 A_{1,2} A_{1,9,26,24} A_{1,3}} \Psi_0^{(0)} + \frac{\gamma^4 A_{1,2}^{1/2} A_{1,4}^{1/2} A_{-1,2,-1}}{4 A_{1,5} A_{1,9,26,24} A_{1,3}^3} \Psi_1^{(0)}$$
$$- \frac{3\gamma^4 A_{1,4}^{1/2} A_{1,6}^{1/2} A_{1,2} A_{-1,2,-1}}{8 A_{1,3} A_{1,12,35} A_{1,15,74,120} A_{1,5}^2} \Psi_3^{(0)}$$
$$+ \frac{3\gamma^4 A_{1,4}^{1/2} A_{1,8}^{1/2} A_{1,2} A_{1,3}}{8 A_{1,5} A_{1,6} A_{1,9,20} A_{1,21,146,336}} \Psi_4^{(0)}. \tag{A3c}$$

(4) The mode (3,0)

$$\Psi_3^{(0)} = -\sqrt{\frac{A_{1,6}}{\gamma\pi}}\left(1 - \frac{3A_{1,3}}{\gamma}\bar{r}^2 + \frac{3A_{1,3} A_{1,4}}{2\gamma^2}\bar{r}^4 - \frac{A_{1,3} A_{1,4} A_{1,5}}{6\gamma^3}\bar{r}^6\right), \tag{A4a}$$

$$\Psi_3^{(1)}/\bar{k}^2 = -\frac{3\gamma^2 A_{1,4}^{1/2} A_{1,6}^{1/2} A_{1,2}}{4 A_{1,5} A_{1,15,74,120}} \Psi_2^{(0)} + \frac{\gamma^2 A_{1,6}^{1/2} A_{1,8}^{1/2} A_{1,3}}{A_{1,7} A_{1,21,146,336}} \Psi_4^{(0)} \tag{A4b}$$

$$\Psi_3^{(2)}/\bar{k}^4 = \frac{3\gamma^4 A_{1,2}^{1/2} A_{1,6}^{1/2} A_{1,1}}{16 A_{1,4} A_{1,5} A_{1,7,12} A_{1,11,30}} \Psi_1^{(0)}$$
$$+ \frac{3\gamma^4 A_{1,4}^{1/2} A_{1,6}^{1/2} A_{1,2} A_{-1,2,-1}}{8 A_{1,7} A_{1,5}^2 A_{1,8,15} A_{1,15,74,120}} \Psi_2^{(0)}$$
$$- \frac{\gamma^4 A_{1,6}^{1/2} A_{1,8}^{1/2} A_{1,3} A_{-1,2,-1}}{2 A_{1,5} A_{1,16,63} A_{1,21,146,336} A_{1,7}^2} \Psi_4^{(0)}$$
$$+ \frac{5\gamma^4 A_{1,10}^{1/2} A_{1,6}^{1/2} A_{1,3} A_{1,4}}{8 A_{1,8} A_{1,7} A_{1,13,42} A_{1,27,242,720}} \Psi_5^{(0)}. \tag{A4c}$$

APPENDIX B: EXPLICIT EXPRESSIONS OF $\alpha^{(l)}$, $\beta^{(l)}$, and $\gamma^{(l)}$

$$\alpha^{(0)} = \beta^{(0)} = \gamma^{(0)} = 0, \tag{B1}$$

$$\alpha^{(1)} = -\frac{\partial n^{(0)}}{\partial\tau} - \frac{1}{r}\frac{\partial}{\partial r}(rn^{(0)} u^{(0)}) - \frac{\partial}{\partial\xi}(n^{(0)} w^{(0)}), \tag{B2a}$$

$$\beta^{(1)} = Mc\frac{\partial u^{(0)}}{\partial\xi} - \frac{1}{2}\frac{\partial}{\partial r}[\mu_s'' n^{(0)} n^{(0)}] - \frac{1}{2}M\frac{\partial}{\partial r}(w^{(0)} w^{(0)}), \tag{B2b}$$

$$\gamma^{(1)} = -M\frac{\partial w^{(0)}}{\partial\tau} - \frac{1}{2}\mu_s''\frac{\partial}{\partial\xi}(n^{(0)} n^{(0)}) - \frac{1}{2}M\frac{\partial}{\partial\xi}(w^{(0)} w^{(0)}) \tag{B2c}$$

with a short notation $\mu_s'' = \partial^2\mu_s(n_s)/\partial n_s^2|_{n_s = n_s^{\text{eq}}}$.

*gxhuang@phy.ecnu.edu.cn

[1] S. Giorgini, L. P. Pitaevskii, and S. Stringari, Rev. Mod. Phys. **80**, 1215 (2008) and reference therein.

[2] M. Bartenstein, A. Altmeyer, S. Riedl, S. Jochim, C. Chin, J. H. Denschlag, and R. Grimm, Phys. Rev. Lett. **92**, 203201 (2004).

[3] J. Kinast, S. L. Hemmer, M. E. Gehm, A. Turlapov, and J. E. Thomas, Phys. Rev. Lett. **92**, 150402 (2004); J. Kinast, A. Turlapov, and J. E. Thomas, Phys. Rev. A **70**, 051401(R) (2004).

[4] M. Greiner, C. A. Regal, and D. S. Jin, Phys. Rev. Lett. **94**, 070403 (2005).

[5] A. Altmeyer, S. Riedl, C. Kohstall, M. J. Wright, R. Geursen, M. Bartenstein, C. Chin, J. H. Denschlag, and R. Grimm, Phys. Rev. Lett. **98**, 040401 (2007); M. J. Wright, S. Riedl, A. Altmeyer, C. Kohstall, E. R. Sanchez Guajardo, J. H. Denschlag, and R. Grimm, *ibid.* **99**, 150403 (2007); A. Altmeyer, S. Riedl, M. J. Wright, C. Kohstall, J. H. Denschlag, and R. Grimm, Phys. Rev. A **76**, 033610 (2007).

[6] C. Menotti, P. Pedri, and S. Stringari, Phys. Rev. Lett. **89**, 250402 (2002).

[7] S. Stringari, Europhys. Lett. **65**, 749 (2004).

[8] H. Heiselberg, Phys. Rev. Lett. **93**, 040402 (2004).

[9] H. Hu, A. Minguzzi, X.-J. Liu, and M. P. Tosi, Phys. Rev. Lett. **93**, 190403 (2004).

[10] D. S. Petrov, Phys. Rev. A **67**, 010703(R) (2003).

[11] R. Combescot and X. Leyronas, Phys. Rev. Lett. **93**, 138901 (2004); R. Combescot, M. Y. Kagan, and S. Stringari, Phys. Rev. A **74**, 042717 (2006).

[12] A. Bulgac and G. F. Bertsch, Phys. Rev. Lett. **94**, 070401 (2005).

[13] T. N. De Silva and E. J. Mueller, Phys. Rev. A **72**, 063614 (2005).

[14] E. Taylor, A. Griffin, N. Fukushima, and Y. Ohashi, Phys. Rev. A **74**, 063626 (2006).

[15] Y. E. Kim and A. L. Zubarev, Phys. Rev. A **70**, 033612 (2004); **72**, 011603(R) (2005).

[16] N. Manini and L. Salasnich, Phys. Rev. A **71**, 033625 (2005).

[17] J. Yin, Y.-L. Ma, and G. Huang, Phys. Rev. A **74**, 013609 (2006).

[18] Y.-L. Ma and G. Huang, Phys. Rev. A **75**, 063629 (2007).

[19] Y. Zhou and G. Huang, Phys. Rev. A **75**, 023611 (2007).

[20] Y. Zhou, W. Wen, and G. Huang, Phys. Rev. B **77**, 104527 (2008).

[21] S. Cao, Y.-l. Ma, and G. Huang, Phys. Rev. A **79**, 013620 (2009).

[22] A. L. Zubarev, J. Phys. B **42**, 011001 (2009).

[23] L. P. Pitaevskii, S. Stringari, and G. Orso, Phys. Rev. A **71**, 053602 (2005).

[24] T. K. Ghosh and K. Machida, Phys. Rev. A **73**, 013613 (2006).

[25] P. Capuzzi, P. Vignolo, F. Federici, and M. P. Tosi, Phys. Rev. A **73**, 021603(R) (2006).

[26] D. E. Miller, J. K. Chin, C. A. Stan, Y. Liu, W. Setiawan, C. Sanner, and W. Ketterle, Phys. Rev. Lett. **99**, 070402 (2007).

[27] Y. He, Q. Chen, C.-C. Chien, and K. Levin, Phys. Rev. A **76**, 051602(R) (2007).

[28] J. Joseph, B. Clancy, L. Luo, J. Kinast, A. Turlapov, and J. E. Thomas, Phys. Rev. Lett. **98**, 170401 (2007).

[29] M. W. Zwierlein, J. R. Abo-Shaeer, A. Schirotzek, C. H. Schunck, and W. Ketterle, Nature (London) **435**, 1047 (2005).

[30] W. Wen, Y. Zhou, and G. Huang, Phys. Rev. A **77**, 033623 (2008).

[31] M. Antezza, F. Dalfovo, L. P. Pitaevskii, and S. Stringari, Phys. Rev. A **76**, 043610 (2007).

[32] W. Wen and G. Huang, Phys. Rev. A **79**, 023605 (2009).

[33] L. Salasnich, N. Manini, and F. Toigo, Phys. Rev. A **77**, 043609 (2008).

[34] P. Pieri and G. C. Strinati, Phys. Rev. Lett. **91**, 030401 (2003).

[35] G. Huang, M. G. Velarde, and V. A. Makarov, Phys. Rev. A **64**, 013617 (2001).

[36] G. Huang, J. Szeftel, and S. Zhu, Phys. Rev. A **65**, 053605 (2002).

[37] G. Huang, V. A. Makarov, and M. G. Velarde, Phys. Rev. A **67**, 023604 (2003).

[38] G. Huang, L. Deng, and Chao Hang, Phys. Rev. E **72**, 036621 (2005).

[39] The critical atom-pair number for a quasi-two-dimensional condensate can also be obtained in a similar way, but it is not needed and thus omitted here.

[40] E. Zaremba, Phys. Rev. A **57**, 518 (1998).

[41] See the Eq. (5) of Ref. 25.

[42] P. Capuzzi, P. Vignolo, F. Federici, and M. P. Tosi, Phys. Rev. A **74**, 057601 (2006).

[43] A multimode dispersion can also occur if many radial modes are excited simultaneously by initial condition, which is not discussed here.

[44] M. J. Ablowitz and H. Segur, *Solitons and Inverse Scattering Transform* (SIAM, Philadelphia, 1981).

[45] G. Huang (unpublished).

[46] A. D. Jackson, G. M. Kavoulakis, and C. J. Pethick, Phys. Rev. A **58**, 2417 (1998).

[47] M. R. Andrews, D. M. Kurn, H.-J. Miesner, D. S. Durfee, C. G. Townsend, S. Inouye, and W. Ketterle, Phys. Rev. Lett. **79**, 553 (1997).